A Two-Dimensional Linear Assumed Strain Triangular Element for Finite Deformation Analysis

Fernando G. Flores
Department of Structures,
National University of Cordoba,
Casilla de correos 916,
5000 Cordoba, Argentina
e-mail: fflores@efn.uncor.edu

An assumed strain approach for a linear triangular element able to handle finite deformation problems is presented in this paper. The element is based on a total Lagrangian formulation and its geometry is defined by three nodes with only translational degrees of freedom. The strains are computed from the metric tensor, which is interpolated linearly from the values obtained at the mid-side points of the element. The evaluation of the gradient at each side of the triangle is made resorting to the geometry of the adjacent elements, leading to a four element patch. The approach is then nonconforming, nevertheless the element passes the patch test. To deal with plasticity at finite deformations a logarithmic stress-strain pair is used where an additive decomposition of elastic and plastic strains is adopted. A hyper-elastic model for the elastic linear stress-strain relation and an isotropic quadratic yield function (Mises) for the plastic part are considered. The element has been implemented in two finite element codes: an implicit static/dynamic program for moderately non-linear problems and an explicit dynamic code for problems with strong nonlinearities. Several examples are shown to assess the behavior of the present element in linear plane stress states and non-linear plane strain states as well as in axi-symmetric problems. [DOI: 10.1115/1.2173674]

1 Introduction

For practical industrial applications in the finite strain range, low order elements are almost exclusively used, specially in problems including contact. Also elements including only physical degrees of freedom are normally preferred. For two-dimensional problems these two aspects restrict the choice to linear triangles and bilinear quadrilaterals.

If only elements with translational degrees of freedom are considered, the linear triangle (constant strain triangle with six degrees of freedom) is not a good choice because it requires very fine meshes to obtain results of engineering precision, and also because it locks for quasi-incompressible problems, e.g., material models including J_2 plasticity or rubber-like materials in plane strain.

From the point of view of the present techniques for finite element development, the bilinear quadrilateral shows much more possibilities. Important efforts have been made in the past 30 years to obtain efficient and robust quadrilaterals which do not lock in the incompressible limit, or have a good performance in bending-dominated problems even with coarse meshes. Different practical approaches and their theoretical basis have been proposed in this direction, from the addition of incompatible modes to improving bending behavior or selective integration of the volumetric response to avoid locking, to the present more refined techniques of assumed strain and enhanced strain finite elements (see, for example, Refs. [1,2] and references listed therein).

From the point of view of industrial applications, the use of triangular elements is more convenient. This is mainly associated with the fact that mesh generators using triangles are more efficient and robust than those using quadrilaterals. This facility is especially important in processes in which large distortions of the original mesh are expected leading unavoidably to remeshing and/or to adaptive refinement.

These reasons have led to the developments of triangles with degrees of freedom that are not strictly displacements, including mixed or hybrid elements on one side and elements with drilling rotations or displacement derivatives on the other side. The extra degrees of freedom in mixed/hybrid (assumed stress) approaches have no associated mass, requiring special time integration techniques [3] when explicit integrators are used. This aspect is important in problems including strong nonlinearities, in which explicit integrators are more robust and preferred. Besides, the standard algorithmic framework for non-linear solid mechanics is typically *strain driven* and, from a practical perspective, algorithms for assumed stress elements are more involved. Elements with drilling freedoms are less common, and have been restricted to plane stress problems [4]. More recently an F-bar method (volumetric strain averaging) [5] that alleviates volumetric locking and an application of sub-grid scales in mixed elements [6] that avoids pressure oscillations were proposed, but none of them improve the poor in-plane behavior of the constant strain triangle.

In this paper a triangular element defined by only three nodes and with only translational degrees of freedom is presented. For the computation of the strains a four element patch including the three adjacent elements is used. This approach has a geometric definition similar to that used in Ref. [7] for the evaluation of the curvatures in a shell element and shares some aspects with the subdivision approach recently proposed for surfaces [8]. The proposed approach linearly interpolates the metric tensor evaluated at the midpoint of each side. The present development is intended to deal with elastic-plastic models at finite strains.

The outline of the paper is as follows. In Sec. 2, the essential governing equations for non-linear solid mechanics relevant to this work are presented. The next two sections are devoted to the finite element approximation: in Sec. 3 the original approach to

Contributed by the Applied Mechanics Division of ASME for publication in the JOURNAL OF APPLIED MECHANICS. Manuscript received June 8, 2005; final manuscript received December 19, 2005. Review conducted by G. C. Buscaglia. Discussion on the paper should be addressed to the Editor, Prof. Robert M. McMeeking, Journal of Applied Mechanics, Department of Mechanical and Environmental Engineering, University of California—Santa Barbara, Santa Barbara, CA 93106-5070, and will be accepted until four months after final publication of the paper itself in the ASME JOURNAL OF APPLIED MECHANICS.

the evaluation of the deformation gradient and the metric tensor is presented, while in Sec. 4 the stiffness matrix necessary for implicit algorithms is derived. Section 5 describes the element performance in linear plane stress problems, and Sec. 6 shows preliminary results for plane strain and axisymmetric problems in the non-linear range. Finally, some conclusions are drawn in Sec. 7.

2 Solid Kinematics

The most relevant aspects associated with the kinematic response of solids are initially presented. More detailed developments can be found in the literature devoted to the field [9].

Consider a solid with reference configuration Ω^0 in R^3 at the initial time $t=0$. Let us then denote with $\mathbf{X} \in \Omega^0$ the position vector of a material point that transforms to a point $\mathbf{x}$ at a time t, both referred to a fixed set of axis.

At each point $\mathbf{X}$ the deformation gradient is defined as

$$\mathbf{F}(\mathbf{X}) = \left[\frac{\partial \mathbf{x}}{\partial X_1}, \frac{\partial \mathbf{x}}{\partial X_2}, \frac{\partial \mathbf{x}}{\partial X_3} \right] = [\mathbf{a}_1\ \mathbf{a}_2\ \mathbf{a}_3] \tag{1}$$

The definition of the Lagrangian tensor $\mathbf{C}=\mathbf{F}^T\mathbf{F}=\mathbf{U}^2$ (with $\mathbf{U}$ the right stretch tensor, and $\mathbf{C}$ the right Cauchy–Green tensor, respectively) allows the introduction of the covariant metric tensor at each point

$$C_{\alpha\beta} = (U^2)_{\alpha\beta} = \mathbf{a}_\alpha \cdot \mathbf{a}_\beta = a_{\alpha\beta} \tag{2}$$

One advantage of the Lagrangian strains is that they are referred to material fibers leading to a simple handling of anisotropic materials. With $\mathbf{U}^2$ it is possible to define different Lagrangian strain measures. With this objective the spectral decomposition is performed as

$$\mathbf{U} = \sum_{\alpha=1}^{3} \lambda_\alpha \mathbf{r}_\alpha \otimes \mathbf{r}_\alpha \tag{3}$$

where λ_α and $\mathbf{r}_\alpha$ are the eigenvalues and eigenvectors, respectively, of the right stretch tensor $\mathbf{U}$.

To deal with plasticity at finite deformations an adequate stress-strain pair must be used. Here a logarithmic (Hencky) strain measure is adopted that, restricted to two-dimensional problems, can be explicitly expressed as

$$\mathbf{E}_{\ln} = \begin{bmatrix} \varepsilon_{11} & \varepsilon_{21} & 0 \\ \varepsilon_{12} & \varepsilon_{22} & 0 \\ 0 & 0 & \varepsilon_{33} \end{bmatrix} = \sum_{\alpha=1}^{3} \ln(\lambda_\alpha) \mathbf{r}_\alpha \otimes \mathbf{r}_\alpha \tag{4}$$

The conjugated stress measure $\mathbf{T}$ is used consistently. Besides this, in the framework of a total Lagrangian formulation, it may be convenient to work with the second Piola–Kirchhoff stress tensor ($\mathbf{S}$) for the residual force evaluation. The relation between the stress $\mathbf{T}$ and the stress $\mathbf{S}$ results from the definition of the rotated tensors

$$\mathbf{T}_L = \mathbf{R}_L^T \mathbf{T} \mathbf{R}_L \tag{5}$$

$$\mathbf{S}_L = \mathbf{R}_L^T \mathbf{S} \mathbf{R}_L \tag{6}$$

where $\mathbf{R}_L$ is the material rotation tensor associated with the principal stretches (eigenvectors of $\mathbf{U}$)

$$\mathbf{R}_L = [\mathbf{r}_1\ \mathbf{r}_2\ \mathbf{r}_3] \tag{7}$$

The relations between these rotated stress measures are

$$[S_L]_{\alpha\alpha} = \frac{1}{\lambda_\alpha^2} [T_L]_{\alpha\alpha} \tag{8}$$

$$[S_L]_{\alpha\beta} = \frac{\ln(\lambda_\alpha/\lambda_\beta)}{\frac{1}{2}(\lambda_\alpha^2 - \lambda_\beta^2)} [T_L]_{\alpha\beta} \tag{9}$$

They allow to compute

$$\mathbf{S} = \mathbf{R}_L \mathbf{S}_L \mathbf{R}_L^T \tag{10}$$

With the previous definitions, the weak form of the equilibrium equations in the reference configuration can be written as

$$\delta\Pi = \int_{\Omega^0} [\delta \mathbf{E}_{\mathrm{GL}} : \mathbf{S}] d\Omega^0 + \delta\Pi_{\mathrm{ext}} = 0 \tag{11}$$

where $\mathbf{E}_{\mathrm{GL}}$ are the Green–Lagrange strains conjugated to $\mathbf{S}$

$$\mathbf{E}_{\mathrm{GL}} = \sum_{\alpha=1}^{3} \frac{1}{2}(\lambda_\alpha^2 - 1) \mathbf{r}_\alpha \otimes \mathbf{r}_\alpha = \frac{1}{2}(\mathbf{U}^2 - \mathbf{1}) \tag{12}$$

Note that the stress-strain pair $\mathbf{S}-\mathbf{E}_{\mathrm{GL}}$ is used only to write the equilibrium equations in the reference configuration. Alternatively, an equivalent formulation to Eq. (11) using the spatial Kirchhoff stress tensor $\boldsymbol{\tau}$ on the actual configuration can be developed.

The constitutive model used in the numerical experiments below corresponds to an elastic-plastic material associated with a ductile metal. For this kind of material, where elastic strains are small and a logarithmic strain measure is used, it seems reasonable to adopt an additive decomposition of elastic and plastic strains $\mathbf{E}_{\ln}^e = \mathbf{E}_{\ln} - \mathbf{E}_{\ln}^p$, where plastic strains may be associated with a plastic deformation gradient $\mathbf{F}^p$ through

$$\mathbf{E}_{\ln}^p = \ln(\mathbf{F}^{pT} \mathbf{F}^p)^{1/2} \tag{13}$$

usually associated with a stress free intermediate configuration. For moderately large shear plastic strains, the results obtained with the additive formulation are similar to those obtained with the multiplicative decomposition of $\mathbf{F}$. See Ref. [10] for a comparison of results for both approaches. An associative Mises yield function (J_2) with non-linear isotropic hardening is considered. Also an anisotropic Hill-type function can be easily defined since the elastic strains are computed on the material axis. The elastic-plastic constitutive equations are integrated using a standard return mapping algorithm.

For the elastic part, a linear relation (constant) between stresses and elastic strains is also adopted. The constitutive relation is split into its deviatoric and volumetric components and in the numerical implementation the volumetric part is averaged at the element center to avoid volumetric locking.

3 Mapping Functions and Gradient Evaluation

In this approach we start from a three-node triangular finite element mesh of the domain. But in contrast with standard finite elements, for the evaluation of the deformations at an element, we resort also to the geometry of the adjacent elements to the triangle being considered (see Fig. 1(*a*)). A quadratic geometry is thus defined by the position of the six nodes

$$\mathbf{X} = \sum_{I=1}^{6} N^I \mathbf{X}^I \quad \mathbf{x} = \sum_{I=1}^{6} N^I \mathbf{x}^I \tag{14}$$

In the parametric space (master element) we keep the vertex positions, nodes 1–3, of the central or main triangle (standard linear triangle) which occupy the positions (see Fig. 1(*b*)).

$$(\xi^1, \eta^1) = (0,0), \quad (\xi^2, \eta^2) = (1,0), \quad (\xi^3, \eta^3) = (0,1)$$

while the three extra nodes forming the patch, denoted as 4–6, occupy the positions

$$(\xi^4, \eta^4) = (1,1), \quad (\xi^5, \eta^5) = (-1,1), \quad (\xi^6, \eta^6) = (1,-1).$$

The following set of shape functions can be defined over this quadratic non-standard six node triangle (with $\zeta = 1-\xi-\eta$)

$$N^1 = \zeta + \xi\eta \quad N^2 = \xi + \eta\zeta \quad N^3 = \eta + \zeta\xi$$

$$N^4 = \frac{\zeta}{2}(\zeta - 1) \quad N^5 = \frac{\xi}{2}(\xi - 1) \quad N^6 = \frac{\eta}{2}(\eta - 1) \tag{15}$$

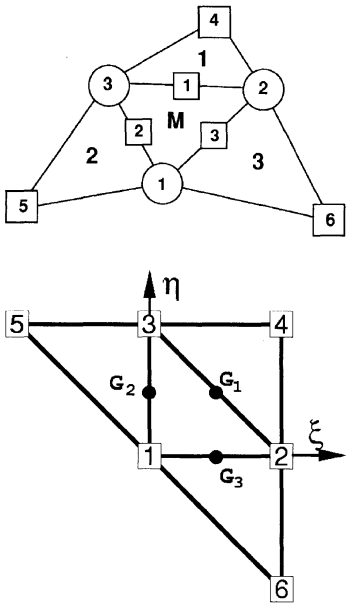

Fig. 1 Patch of elements (*a*) in spatial coordinates, (*b*) in natural coordinates

The aim of this mapping is the computation of the metric tensor at selected points in the central element to generate an assumed strain approach. For a linear interpolation in local natural coordinates three values are needed. The points used for evaluation are located at the middle of each side of the reference triangle (**M** in Fig. 1(*a*)). They are indicated as G_1, G_2 and G_3 in Fig. 1(*b*). This choice has the following properties:

- The gradient computed at each mid-side point depends exclusively on the positions of the nodes associated with the two elements adjacent to the side. This can be immediately checked by differentiating the shape functions and evaluating at the middle of each side.
- When the deformation gradients are computed at the common side of two neighbor triangles, the same four nodes will be used. Thus, at each side of the mesh, a unique deformation gradient exists.

The deformation gradient is then determined by the coordinates of a patch of four elements, which includes the element under consideration (**M** in Fig. 1(*a*)) as the central one. Note that the present approach is nonconforming because the quadratic geometry computed from two adjacent triangles is different along the common side.

Once the deformation gradient has been defined the derivation is standard, and some details are given in the sequel. We will denote by $\mathbf{t}_1$ and $\mathbf{t}_2$ the two orthogonal unit vectors in a local Cartesian system conveniently selected (e.g., the orthotropic principal directions of the constitutive material). The natural derivatives of the reference coordinates allow to compute the Jacobian matrix of the isoparametric mapping $\mathbf{J}$ and the Cartesian derivatives of the shape functions $N_1^I N_2^I$. With them the deformation gradient at the deformed configuration (respect to the original Cartesian system) can be computed as

$$[\mathbf{x}_{,1}, \mathbf{x}_{,2}] = [\mathbf{x}_{,\xi}, \mathbf{x}_{,\eta}]\mathbf{J}^{-1} \tag{16}$$

and the (in-plane) covariant metric tensor

$$\mathbf{C} = \begin{bmatrix} a_{11} & a_{12} \\ a_{21} & a_{22} \end{bmatrix} = \begin{bmatrix} \mathbf{x}_{,1}\cdot\mathbf{x}_{,1} & \mathbf{x}_{,1}\cdot\mathbf{x}_{,2} \\ \mathbf{x}_{,2}\cdot\mathbf{x}_{,1} & \mathbf{x}_{,2}\cdot\mathbf{x}_{,2} \end{bmatrix} \tag{17}$$

and finally any in-plane desired Lagrangian strain measure. For example, the Green–Lagrange strain tensor

$$\mathbf{E}_{\mathrm{GL}} = \frac{1}{2}\begin{bmatrix} \mathbf{x}_{,1}\cdot\mathbf{x}_{,1}-1 & \mathbf{x}_{,1}\cdot\mathbf{x}_{,2} \\ \mathbf{x}_{,2}\cdot\mathbf{x}_{,1} & \mathbf{x}_{,2}\cdot\mathbf{x}_{,2}-1 \end{bmatrix} = \frac{1}{2}\begin{bmatrix} a_{11}-1 & a_{12} \\ a_{21} & a_{22}-1 \end{bmatrix} \tag{18}$$

An element that has a side along the boundary does not have an adjacent element on this side. In this case the deformation gradient at this side is computed as the gradient of the central element using the standard linear interpolation. Once the metric tensor ($\mathbf{C}_i$) is computed at each mid-side point i, the element can be classified as an **assumed strain** element if the metric tensor is interpolated as a function of the computed values at the sides. This allows to associate a theoretical basis to the present approach.

$$\mathbf{C}(\xi,\eta) = (1-2\zeta)\mathbf{C}_1 + (1-2\xi)\mathbf{C}_2 + (1-2\eta)\mathbf{C}_3 \tag{19}$$

4 Stiffness Matrix

The derivative of the weak form (Eq. (11)) is needed for most of the implicit predictor-corrector algorithms. As usual, for nonlinear problems, the **material** and **geometric** parts are considered separately. The material part is almost standard and does not offer difficulties, it is the result of the integral

$$\delta\mathbf{u}^T\mathbf{K}_M\Delta\mathbf{u} = \delta\mathbf{u}^T\int_A \mathbf{B}^T\mathbf{D}\mathbf{B}dA\Delta\mathbf{u} \tag{20}$$

where matrix **B** results from the evaluation of the variation of the Green–Lagrange strain tensor (Eq. (18)). In the numerical implementation, adequate changes must be introduced for elements on the boundary. Matrix **D** is the tangent elasticity matrix or, in elastic-plastic problems, the tangent/algorithmic constitutive matrix $\mathbf{D}_{\mathrm{ep}}$.

The geometric part turns out from

$$\delta\mathbf{u}^T\mathbf{K}_G\Delta\mathbf{u} = \int_A \frac{\partial}{\partial\mathbf{u}}(\delta\mathbf{E}_{\mathrm{GL}}^T\mathbf{S})\Delta\mathbf{u}dA \tag{21}$$

which can be obtained by adding the contributions from the three mid-side points (written in matrix form):

$$\delta\mathbf{u}^T\mathbf{K}_G\Delta\mathbf{u} = \frac{1}{3}\sum_{K=1}^{3}\sum_{I=1}^{4}\sum_{J=1}^{4}\left\{\delta\mathbf{u}^I\int_A [N^J_{,1}\ N^J_{,2}]\begin{bmatrix} S_{11} & S_{12} \\ S_{21} & S_{22}\end{bmatrix} \times \begin{bmatrix} N^J_{,1} \\ N^J_{,2}\end{bmatrix} dA\Delta\mathbf{u}^J\right\}^{(K)} \tag{22}$$

where index $K=1,3$ is the side and $N^{I(K)}$ are the shape functions restricted to the four contributing nodes at each point ($I,J=1,4$).

In the numerical comparisons we denote by TR3 the present element when three points are used to integrate the deviatoric forces and corresponding stiffness matrix. And by TR1 when only one integration point is used, equivalent to averaging the metric tensors computed at each side. The latter is the usual case because it needs less storage for internal variables; it is more competitive for explicit codes and does not have spurious modes.

For the TR1 version the computational cost is slightly above the standard constant strain triangle (CST). Two aspects must be considered: (a) the evaluation of the internal forces, (b) the computations associated to the stiffness matrix. For codes with explicit integration of the momentum equations only the former is concerned, while for implicit integrators the latter is the most relevant. For the evaluation of the internal forces the differences with the CST amount to the computation of the average metric tensor (or the deformation gradient) than can be made quite efficiently. The same also applies to the stiffness matrix evaluation. It must be noted that also a slightly wider bandwidth will be obtained leading to higher CPU times to solve the equations systems.

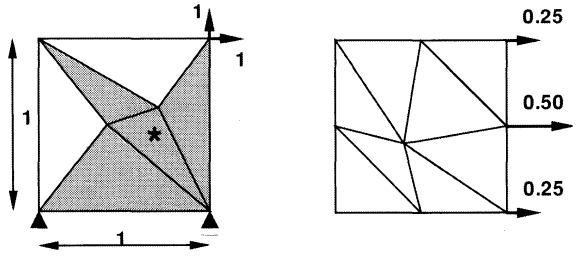

Fig. 2 Membrane patch test

5 Linear Numerical Examples

In this section and the next, a summary of the numerical experiments performed to assess the behavior of this element is presented. In this section linear problems in plane stress state are considered. An implicit static/dynamic program for moderately non-linear simulations developed by the author is used. For comparisons, the results obtained with other elements are included, namely: the constant strain triangle (CST), the linear strain triangle (LST) and three three-node triangles (ALL-3I, BER-85 and CF-OPT) with three degrees of freedom per node (both displacements and the drilling rotation) obtained with different formulations as reported in Ref. [4]. With ALL-3I we denote the element developed by Allman [11] integrated with three inner points; with BER-85 we denote the element developed by Bergan [12] using the free formulation and with CF-OPT we denote the element developed by Felippa and Militello based on the ANDES scheme [13] optimized to reproduce exactly constant bending states.

5.1 Membrane Patch Test. As the present approach is non-conforming, one of main aspects to be considered is the satisfaction of the patch test. To assess this a square domain of unit side subjected to nodal forces associated with a uniform unit stress state (both Cartesian directions and shear) have been used. Two possible patches of elements are shown in Fig. 2. In the first patch, the loads necessary to obtain a uniform stress state $S_{xx}=S_{xy}=S_{yy}=1$ are shown. In the second patch, only the loads corresponding to a uniform traction in the direction x are depicted. For both meshes unitary stresses are obtained at all elements, using one or three integration points.

Two very important things may be noted in this simple example. First, in the second case, note that the nodal forces are the loads associated with the linear triangle and not to the quadratic one. This has important implications in problems including contact, where the use of the standard LST implies non-uniform equivalent nodal forces for a uniform pressure leading to the well-known problems of quadratic elements in contact simulations. Second, note that the element patches used for gradient computations at each element are quite distorted. In the first mesh the element patch used to compute strains at element * is shaded as an example. A LST element defined with the same six points will show a very strong sensitivity to such distortion leading to unpredictable results.

5.2 Short Cantilever Under Uniform Shear. This example (see Fig. 3), taken from Ref. [4], is used to assess the behavior and

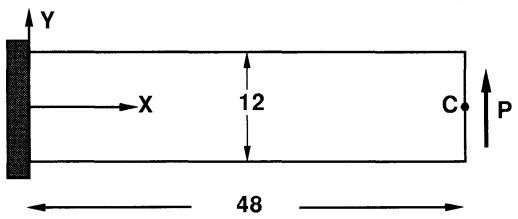

Fig. 3 Shear loaded short cantilever: no contraction allowed at the root. E=30,000, ν=0.25, h=1.

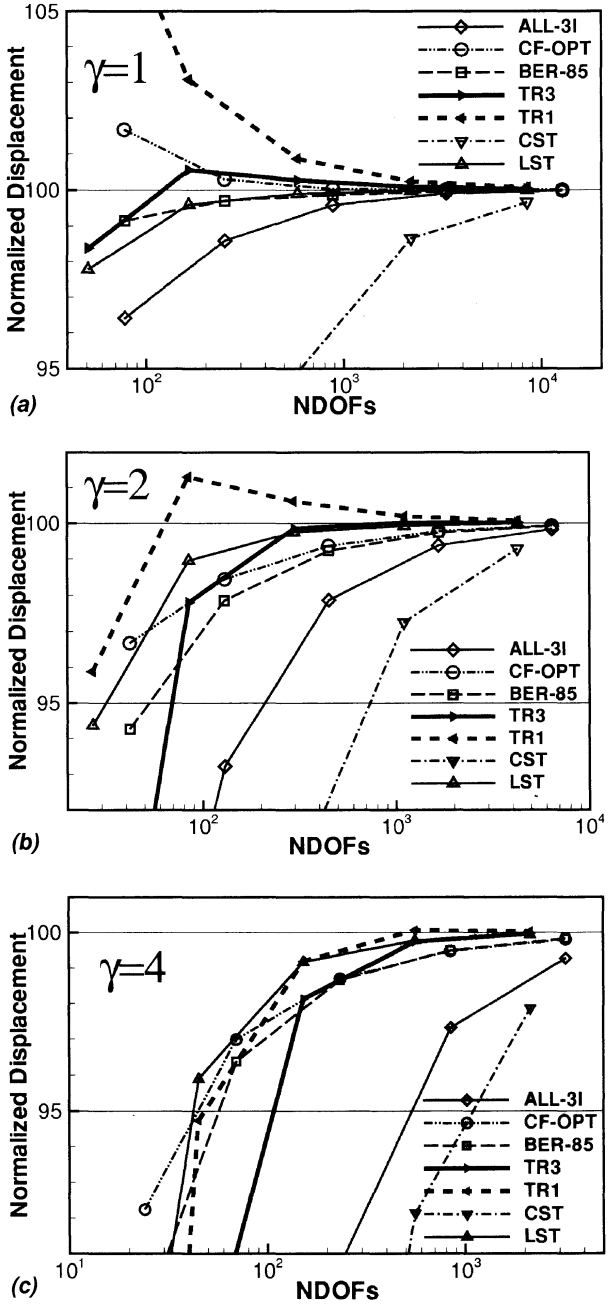

Fig. 4 Tip deflections for short cantilever under end load. (*a*) γ=1, (*b*) γ=2, (*c*) γ=4.

convergence properties of elements under bending and shear when the element aspect ratio is increased. Shear load is parabolically distributed according to beam theory. All displacements are constrained at the root, not allowing Poisson's contraction. A numerically converged solution of the deflection at point **C** of δ_C =0.35601 is used for normalization. Mesh units are formed by four half-thickness overlaid triangles to avoid orientation influence. Along direction y (beam height) 2, 4, 8, 16, and 32 mesh units are considered while along direction x mesh is defined by element aspect ratio values γ=1, 2, and 4.

The results for the vertical displacements of point **C** are plotted in Figs. 4(*a*)–4(*c*) for the three element aspect ratios and for all the elements described above. In all the cases the best results are obtained with the linear strain triangle while the constant strain triangle is notoriously overstiff. The performance of elements with drilling freedom deteriorates as the aspect ratio increases, specially Allman's triangle. Present element fully integrated (TR3) converges rapidly and is less sensitive to aspect ratio than ele-

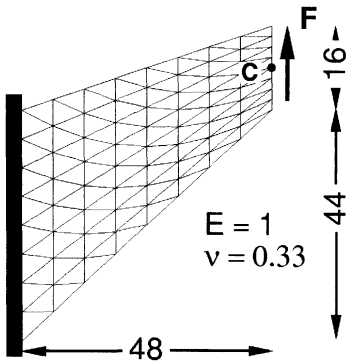

Fig. 5 Cook's membrane problem. Geometry and load.

ments with drilling freedoms. Present element with only one integration point (TR1) is slightly more flexible but converges to the correct solution.

5.3 Cook's Membrane Problem. One of the main targets of this proposal is to obtain a membrane approach with a behavior similar to the linear strain triangle in arbitrary domains. Such capacity is studied in this example [14], corresponding to a problem with an important amount of shear energy involved, intended also to assess the ability of the element to distort. Figure 5 shows the geometry of a tapered panel clamped on one side and with a uniformly distributed shear load on the opposite side. In Fig. 6 the vertical displacement of point **C** (midpoint of the loaded side) for the uniformly refined meshes considered are plotted as a function of the total number of degrees of freedom.

For the present element with three integration points, it can be seen that for the coarsest mesh (two linear elements), the measured displacement is slightly superior than the constant strain triangle; but when the mesh is refined, the values computed rapidly catch up with those obtained with the linear strain triangle. For the elements with drilling freedoms, the trends of the previous example are reverted. The more general Allman's element has a better performance than the other two (optimized for uniform bending) which give similar values and converge slower. The present element with only one integration point (TR1) shows excellent predictions for coarse meshes and fast convergence properties.

6 Nonlinear Numerical Examples

In this second part of the numerical experiments, examples in the geometric and material non-linear range are discussed. Due to the characteristics of the problems modeled, including strong nonlinearities and contact with friction, a program with explicit integration of the governing equations was used [15]. This program

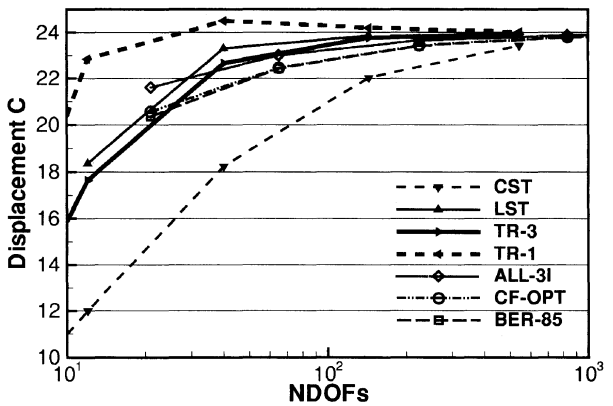

Fig. 6 Cook's membrane problem. Vertical deflections of point C (plane stress).

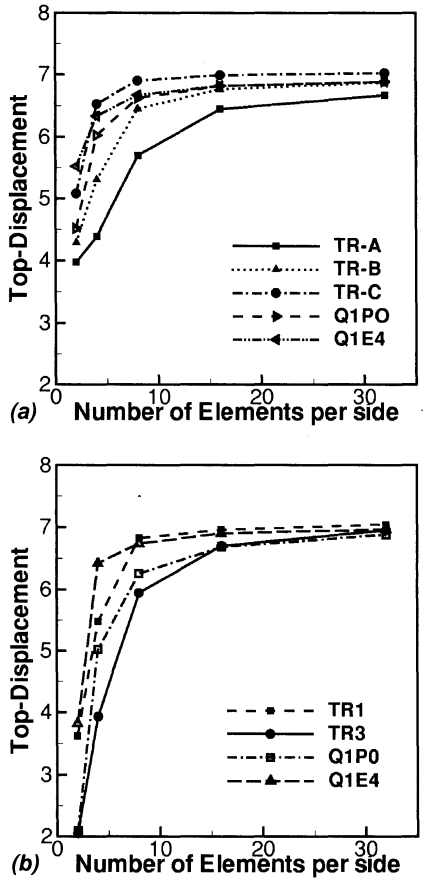

Fig. 7 Cook's problem in plane strain. Convergence of finite element solutions. (*a*) quasi-incompressible finite elasticity. (*b*) Finite Strain J_2 flow theory.

allows to obtain pseudo-static solutions using dynamic relaxation. The problems analyzed in this second part are in plane strain or axisymmetric states. Special emphasis is placed in detecting if the element is capable of handling elastic-plastic problems with isochoric plastic flow or quasi-incompressible elastic problems.

6.1 Cook's Problem in Plane Strain. The same geometry considered in Sec. 5.3 is used, but here in a state of plane strain. Two different materials are considered. First, a quasi-incompressible linear elastic material defined by a shear modulus $\mu=80.1938$ GPa and three possible values of the bulk modulus $K_A=401.0\times10^3$ GPa, $K_B=40.1\times10^3$ GPa and $K_C=4.01\times10^3$ GPa in correspondence with three values of the Poisson ratio $\nu=0.4999$, 0.4990, and 0.4900, respectively. Second, an elastic-plastic material defined by the elastic constants $\mu=80.1938$ GPa and $K=164.21$ GPa and J_2 plasticity with nonlinear hardening defined by the yield stress $\sigma_y(e^p)=0.450+0.12924e^p+(0.715-0.450)(1-e^{-16.93e^p})$ [GPa]. The applied load is 100 kN for the elastic case, and 5 kN in the elastic-plastic case.

Figure 7 plots the vertical displacement of the upper corner versus the number of elements per side of the mesh. Figure 7(*a*) corresponds to the quasi-incompressible elastic case using one integration point for present element. Results are shown for the three bulk modulus considered, denoted as TR-A, TR-B, and TR-C. Curve TR-A (Poisson's ratio $\nu=0.4999$) shows clearly a slow convergence. For a Poisson's ratio of $\nu=0.4990$ convergence is reasonably good, while for the lowest considered value of $\nu=0.4900$ convergence is very good, similar to that obtained in the plane stress case. For comparative purposes, results for the highest Poisson's ratio obtained with two four node quadrilaterals are included. Q1P0 [16] is a mixed element equivalent to integrating the volumetric part with one point and the deviatoric part with four

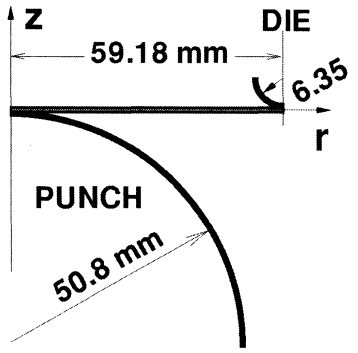

Fig. 8 Stretching of circular sheet with a hemispherical punch

points; Q1EA is an enhanced strain element [17]. Both quadrilaterals show a better performance than the proposed triangle (TR1) for this type of quasi-incompressible elastic problem.

Figure 7(*b*) corresponds to the elastic-plastic material. Results for the two versions (one and three integration points) of the present element and the two quadrilaterals mentioned in the previous paragraph are included. In this case, TR3 shows a stiffer behavior than quadrilaterals, but there is no locking. While the element version TR1 converges faster than both quadrilaterals used for comparison.

6.2 Stretching of a Circular Sheet With a Hemispherical Punch. The last example considered is an axisymmetric problem with moderately large strains. This *benchmark* was proposed in Ref. [18] and has been widely used to test two-dimensional solid elements. The simple geometry of this test is shown in Fig. 8. The sheet thickness is 1 mm and the material is defined by the elastic constants $E=69.004$ GPa and $\nu=0.3$, and J_2 plasticity with an isotropic hardening law $\sigma_y=0.589(10^{-4}+e^p)^{0.216}$ GPa. Contact between the tools and the sheet is modeled using penalization and the friction coefficient adopted is $\mu=0.3$. A uniform mesh of 28 elements in direction r and four elements in the thickness was used ($28\times4\times2$ TR1 elements).

Figure 9(*a*) plots the force on the punch versus the punch travel along the process. These values are in agreement with most of the simulations where solid elements (as opposite to shell elements) have been used, as they can deal with local effects associated with shear distortion due to the small radius of the die and to the frictional contact with the tools [16]. Figure 9(*b*) shows the thickness along the radius for different punch travels, and Fig. 9(*c*) the effective plastic strain on the middle surface of the sheet for different punch travels. These results agree quite well with most of the data published for this benchmark including solid [16] and shell elements [7].

7 Conclusions

A triangular finite element for the simulation of two-dimensional solids has been presented. The geometry is defined by three nodes and only translational degrees of freedom are used, which makes the element convenient for implementation in codes with explicit integration of the governing equations for problems including contact and adaptive remeshing. The element is nonconforming but satisfies the *patch test* and the numerical test computed did not show problems.

In uniform bending plane stress states, the element displays a reasonable behavior. For more general problems including a massive discretization, the element shows a performance similar to the linear strain element. Thus the element turns out to be an excellent candidate for the membrane part of a shell element [19], specially if it is oriented to sheet metal forming, where the membrane behavior is of utmost importance and requires a detailed discretization of the domain.

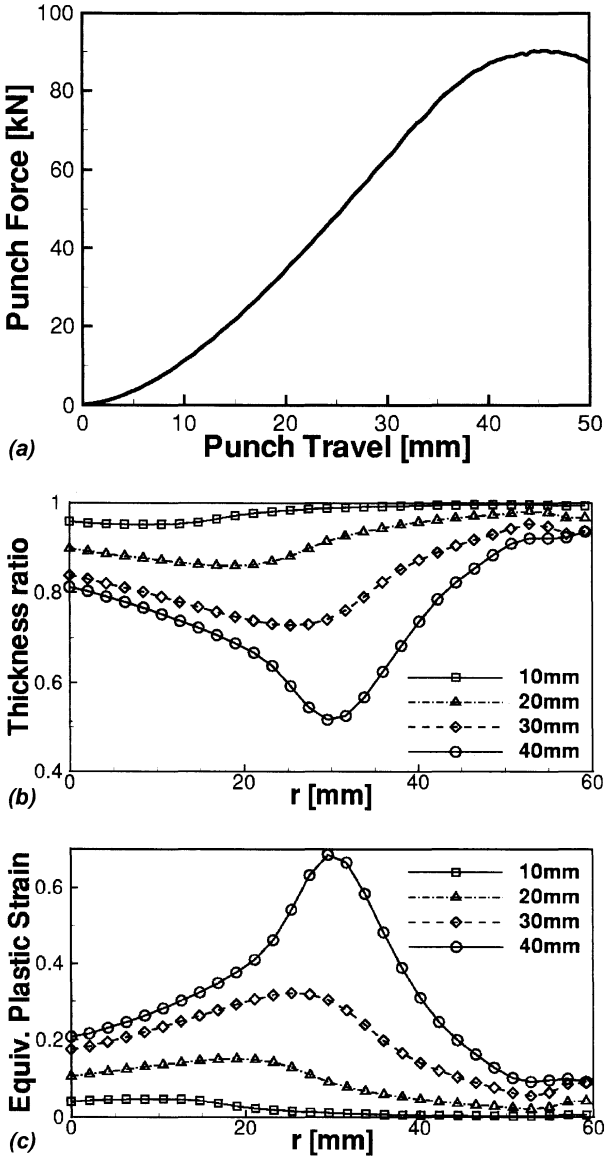

Fig. 9 Stretching of circular sheet with a hemispherical punch. (*a*) Punch force vs punch travel. (*b*) Thickness ratio along the radius for different punch travels. (*c*) Equivalent plastic strain along the radius for different punch travels.

For plane strain and axisymmetric states with finite strains in the plastic range, the element performance is very good, similar to the enhanced strain quadrilaterals. For quasi-incompressible elastic problems the element is rather stiff for Poisson's ratio greater than 0.4999 but is quite good for Poisson's ratio below 0.4990

A more detailed assessment of the element must be performed. In particular the behavior in problems including very large strains (exceeding 1) and the convergence properties in complex domains and meshes where large gradients of the element size exist.

Acknowledgment

The author is a member of the scientific staff of the Science Research Council of Argentina (CONICET). The support provided by grants of CONICET is gratefully acknowledged.

References

[1] Simo, J. C., and Rifai, M. S., 1990, "A Class of Mixed Assumed Strain Methods and the Method of Incompatible Modes," Int. J. Numer. Methods Eng., **29**, pp. 1595–1638.

[2] Armero, F., 2000, "On the Locking and Stability of Finite Elements in Finite Deformations Plane Strain Problems," Comput. Struct., **75**, pp. 261–290.

[3] Zienkiewicz, O. C., Rojek, J., Taylor, R. L., and Pastor, M., 1998, "Triangles and Tetrahedra in Explicit Dynamic Codes for Solids," Int. J. Numer. Methods

Eng., **43**, pp. 565–583.
[4] Felippa, C. A., 2003, "A Study of Optimal Membrane Triangles With Drilling Freedoms," Comput. Methods Appl. Mech. Eng., **192**, pp. 2125–2168.
[5] de Souza Neto, E. A., Andrade Pires, F. M., and Owen, D. R. J., 2005, "F-Bar-Based Linear Triangles and Tetrahedra for Finite Strain Analysis of Nearly Incompressible Solids. Part I: Formulation and Benchmarking," Int. J. Numer. Methods Eng., **62**, pp. 353–383.
[6] Cervera, M., Chiumenti, M., Valverde, Q., and Agelet de Saracibar, C., 2003, "Mixed Linear/Linear Simplicial Elements for Incompressible Elasticity and Plasticity," Comput. Methods Appl. Mech. Eng., **192**, pp. 5249–5263.
[7] Flores, F. G., and Oñate, E., 2001, "A Basic Thin Shell Triangle With Only Translational DOFs for Large Strain Plasticity," Int. J. Numer. Methods Eng., **51**, pp. 57–83.
[8] Cirak, F., and Ortiz, M., 2000, "Subdivision Surfaces: A New Paradigm for Thin-Shell Finite Element Analysis," Int. J. Numer. Methods Eng., **47**, pp. 2039–2072.
[9] Marsden, J. E., and Hughes, T. J. R., 1994, *Mathematical Foundations of Elasticity*, Dover, New York.
[10] Miehe, C., and Apel, N., 2004, "Anisotropic Elastic-Plastic Analysis of Shells at Large Strains. A Comparison of Multiplicative and Additive Approaches to Enhanced Finite Element Design and Constitutive Modelling," Int. J. Numer. Methods Eng., **61**, pp. 2067–2113.
[11] Allman, D. J., 1984, "A Compatible Triangular Element Including Vertex Rotations for Plane Elasticity Analysis," Comput. Struct., **19**, pp. 1–8.
[12] Bergan, P. G., and Felippa, C. A., 1985, "A Triangular Membrane Element With Rotational Degrees of Freedom," Comput. Methods Appl. Mech. Eng., **50**, pp. 25–69.
[13] Felippa, C. A., and Militello, C., 1992, "Membrane Triangles With Corner Drilling Freedoms: II. The ANDES Element," Finite Elem. Anal. Design, **12**, pp. 189–201.
[14] Cook, R. D., 1974, "Improved Two-Dimensional Finite Element," J. Struct. Div. ASCE, **100**, ST6, pp. 1851–1863.
[15] STAMPACK, 2005, *A General Finite Element System for Sheet Stamping and Forming Problems*, Quantech ATZ, Barcelona, Spain, ver. 6.00.
[16] Garino, C. García, 1993, "A Numerical Model for the Analysis of Elastic-Plastic Solids Subjected to Large Strains," Ph.D. thesis (in Spanish) Universidad Politécnica de Cataluña, Barcelona.
[17] Glaser, S., and Armero, F., 1997, "On the Formulation of Enhanced Strain Finite Elements in Finite Deformations," Eng. Comput., **14**, pp. 757–791.
[18] Lee, J. K., Wagoner, R. H., and Nakamachi, E., 1990, "A Benchmark Test for Sheet Metal Forming," Technical Report, Ohio State University.
[19] Flores, F. G., and Oñate, E., 2005, "Improvements in the Membrane Behaviour of the Three Node Rotation-Free BST Shell Triangle Using an Assumed Strain Approach," Comput. Methods Appl. Mech. Eng., **194**, pp. 907–932.